Article

J. Mex. Chem. Soc. **2014**, *58(2),* 95-98

ISSN 1870-249X

The Effect of NaOH and KOH on the Characterization of Mesoporous AlOOH Nanostructures in the Hydrothermal Route

Nahid Haghnazari, Mozaffar Abdollahifar,* and Farahnaz Jahani

Department of Chemical Engineering, Kermanshah Branch, Islamic Azad University, Kermanshah 67131, Iran.
abdollahifar@gmail.com

Received August 26th, 2013; Accepted December 3rd, 2013.

Abstract. Mesoporous AlOOH was synthesized by hydrothermal treatment from aluminium nitrate and NaOH or KOH. The effect of NaOH and KOH as precipitating agents on the characterization of samples were investigated. XRD, FTIR, FESEM and N_2 adsorption-desorption analytical techniques were used to characterize the products. Our results showed that using KOH as precipitating agent was favourable for the formation of mesoporous and crystalline AlOOH with high BET-specific surface area of 98 m^2/g.
Key words: AlOOH, mesoporous, NaOH, KOH, Hydrothermal.

Resumen. El ALOOH mesoporoso fue sintetizado a partir de nitrato de aluminio y NaOH o KOH. Se investigó el efecto de NaOH y KOH como agentes precipitantes en la caracterización de las muestras. Para caracterizar los productos se utilizaron las técnicas XRD, FTIR, FESEM y la absorción-desorción de N_2 como técnicas analíticas. Los resultados muestran que la utilización de KOH como agente precipitante fue favorable para la formación del AlOOH mesoporoso y cristalino, con una superficie específica (BET), de 98 m^2/g.
Palabras clave: AlOOH, mesoporoso, NaOH, KOH.

Introduction

Transition aluminas such as γ-Al_2O_3 and aluminum oxide hydroxide have been commonly used in the field of heterogeneous catalysis, adsorbent, refractory, coatings and abrasives due to their unique properties[1-5], and as well as γ-Al_2O_3 was applied as reinforce of ceramic composites for its low thermal conductivity, high chemical stability and strength, corrosion resistance, and excellent electrical insulation [6, 7]. Transition aluminas are prepared through the calcination of aluminum oxide-hydroxides or hydroxides. Boehmite (AlOOH) or aluminum oxide-hydroxide is an important precursor because the heat treatment of boehmite produces a series of transition aluminas from γ-Al_2O_3 to Δ-Al_2O_3, θ-Al_2O_3 and α-Al_2O_3 with increasing temperature from 400 to 1250 °C [8], which exhibit high surface areas and thermal stability around 1000 °C.

Various methods, such as sol-gel [9], Solvothermal [10], Microwave-Assisted Solvothermal [11], H_2SO_4-assisted hydrothermal [12] and simple hydrothermal method [13-18] were employed for the preparation of AlOOH nanostructures, e.g. nanorods, nanowires, nanoflakes and nanofibers. The hydrothermal route is one of the promising and attractive methods for the synthesis of high-quality nanomaterials, especially AlOOH nanostructures. The reaction condition in the hydrothermal route is easy controllable, and not formed macroscopic agglomeration as well as the samples prepared by this method have good crystallinity [19, 20].

It has been observed that in the hydrothermal method, the shape, physical properties of AlOOH depend on the pH of the solution, precipitating agent, temperature and the residence time in the autoclave [12, 14, 15, 17, 18, 21-23]. In this investigation, we report the effect of precipitating agents in the characterization of new mesoporous and crystalline AlOOH synthesized via the hydrothermal treatment of reaction mixtures containing aluminum nitrate and NaOH or KOH. The products so obtained were characterized and their physical properties like surface area and total pore volume were measured.

Results and Discussions

FTIR and XRD analysis

Fig. 1 shows the FTIR spectrum of samples prepared with NaOH (a) and KOH (b), respectively. As can be seen, for both samples, the intensive bands at 3095 and 3301 cm^{-1} belong to the υ_{as}(Al)O-H and υ_s(Al)O-H stretching vibrations. The two weak bands at 1971 and 2092 cm^{-1} are the combination bands. The absorption edge of the hydroxyl bands on the surface was found at 1638 cm^{-1}. These absorption bands agree precisely with the ones previously reported in the literature [21]. The bands at 1065 cm^{-1} and 1156 cm^{-1} (shoulder) are assigned to

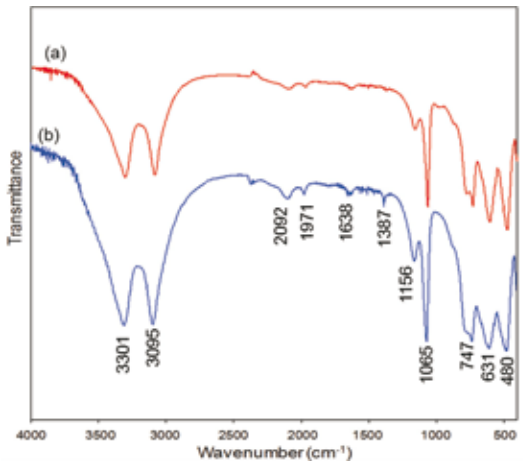

Fig. 1. The effect of NaOH (a) and KOH (b) on the FTIR spectrums of mesoporous AlOOH.

Table 1. AlOOH IR band positions measured on our powders, together with values and assignment from Refs. [8, 21, 22, 24].

Boehmite band position (cm^{-1})		Assignment (from Refs. [8, 21, 22, 24])
This work	from Ref. [8]	
480	491	vibration mode of AlO_6
631	616	
747	740	OH torsional mode
1065	1072	Symmetric and asymmetric bending of AlOH
1156	1160	
1387	1375	H_2O deformation vibrations and or vibration of NO_3
1638		hydroxyl bands on the surface
1971		combination bands
2092		
3095	3090	υ_{as}(Al)O-H and υ_s(Al)O-H stretching vibrations or O-H stretching mode.
3301	3304	

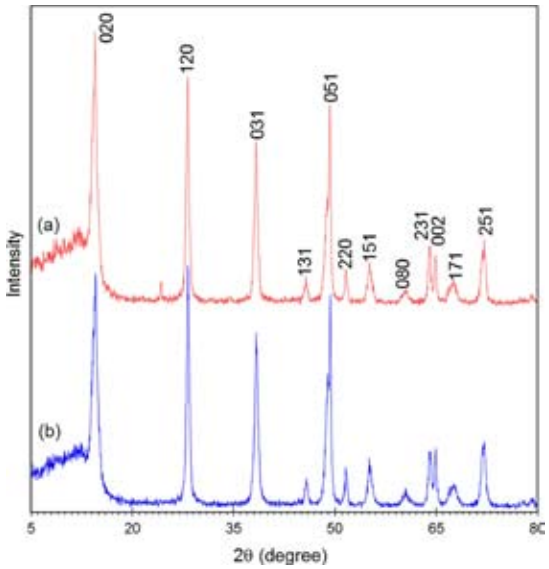

Fig. 2. The effect of NaOH (a) and KOH (b) on the XRD patterns of mesoporous AlOOH.

the Δ_s Al-O-H and Δ_{as} Al-O-H modes of AlOOH, respectively [24]. The three bands at 480 and 631cm^{-1} represent the vibration mode of AlO_6 [22] and the band at 747 cm^{-1} assigned to the OH torsional mode [8]. The band at 1387 cm^{-1} for sample of b is due to the characteristic stretching vibration of NO_3 caused by absorbed nitrates and or H_2O deformation vibrations [8]. The main bands are listed in Table 1, together with their assignment, and compare well with values available in the literature [8, 21, 22, 24].

More characteristics of AlOOH are also observed in their XRD patterns. Fig. 2 shows the XRD patterns of samples prepared with NaOH (a) and KOH (b), respectively. X-ray powder diffraction indicated that both samples were single-phase AlOOH, in accordance with the literature [21]. All the sharp and strong reflection peaks of samples (a) are readily indexed as orthorhombic boehmite (AlOOH, JCPDS Card No. 21-1307, space group Amam 63, unit-cell parameters, a = 3.700, b = 12.227, and c = 2.868 Å at 25 °C.). The essentially same XRD pattern (Fig. 2b) was obtained, even when the sample was prepared by KOH. No obvious XRD peaks assignable to impurities are detected in Fig. 2, indicating the high purity and crystallinity of the as prepared AlOOH samples. The most intense peak is at (020) according to the standard pattern. However, the maximum intensity of the product (a) and (b) were at (020) and (120) peaks, respectively. This phenomenon may be caused by preferential growth along the (120) plane and the kind of precipitating agent. The estimated mean crystallite sizes from the broadening of diffraction lines values using the Scherrer equation are given in Table 2.

Table 2. Crystallite size, estimated from the broadening of diffraction lines of samples.

Sample with precipitating agent	Mean crystallite size (nm)
NaOH	28
KOH	17

FESM analysis

The effect of NaOH and KOH on the morphology of the obtained ALOOH was evaluated using FESEM Fig. 3. Under the reported conditions, for sample (a) clearly displays that AlOOH nanosheets attach together and assemble into nano-architecture and close observation as shown in Fig. 4a reveals that the individual AlOOH nanosheets have a mean thickness of about 25 nm, but for sample (b) both the width and the length nanosheets are much smaller than the previous sample. Fig. 4b shows that the AlOOH nanosheets have a mean thickness of about 14 nm.

N_2 adsorption-desorption analysis

To investigate the effect of NaOH and KOH on the specific surface area and porous nature (pore diameter and volume) of the AlOOH architectures, Brunauer-Emmett-Teller (BET) gas-sorption measurements were carried out. The nitrogen sorption isotherms of the samples prepared with different precipitating agent are shown in Fig. 4. The recorded nitrogen adsorption-desorption isotherms for the samples show a significant hysteresis at relative pressures P/P_0 above 0.65. The hysteresis loops can be identified as type IV, which is characteristic of mesoporous materials [25]. According to the IUPAC classification the hysteresis loop of sample (a) is the H1, but the observed hysteresis loop for sample (b) has intermediate shape between so-called H1 and H2 types [25]. The sample (b) presents a well-defined step in the desorption branch of the isotherm curve at P/P_0 value of 0.88. This is characteristic of capillary condensation within

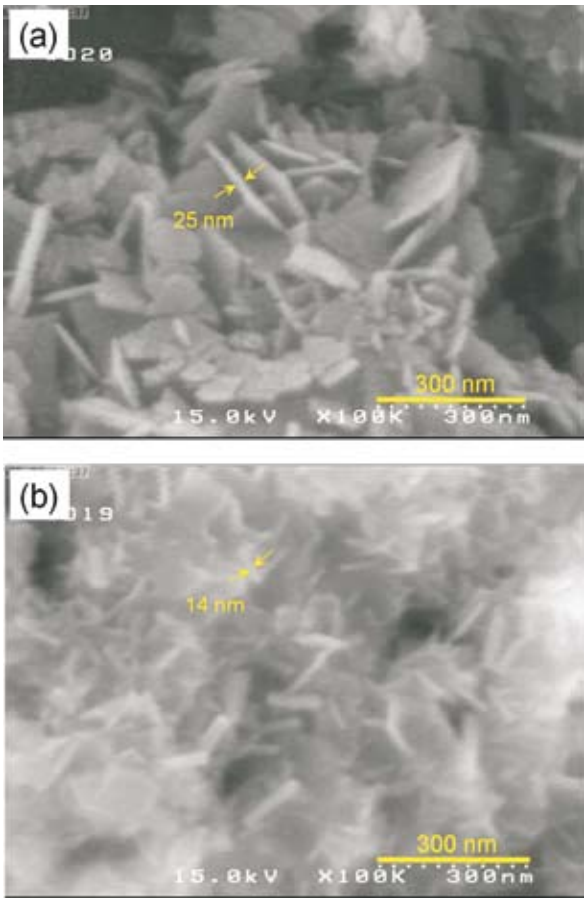

Fig. 3. The effect of NaOH (a) and KOH (b) on the FESEM images of mesoporous AlOOH.

uniform pores and showed a narrower pore size distribution than the sample (a) (Fig. 4, inset).

Interestingly, a change in the synthesis conditions may lead to marked differences in the structural properties. The sample prepared with NaOH has a specific surface area of 79 m^2/g, average pore size of 30 nm and a total pore volume 0.59 cm^3/g whereas the surface areas, average pore size and pore volume of sample prepared with KOH were 98 m^2/g, 18 nm and 0.45 cm^3/g, respectively. According to our results, a trend can be identified. In contrast with NaOH, when the KOH used as precipitating agent, the specific surface area was increased by 24% while the average pore size and total pore volume for the sample decreased by 67 and 31%, respectively. The BET specific surface area of the sample (b) is 98 m^2/g, which was higher, than reported in the literature for crystalline AlOOH [24, 26].

Experimental

Materials and Methods

All chemical reagents were analytical grade and purchased from Scharlau Chemical Reagent Company (Spain) without further

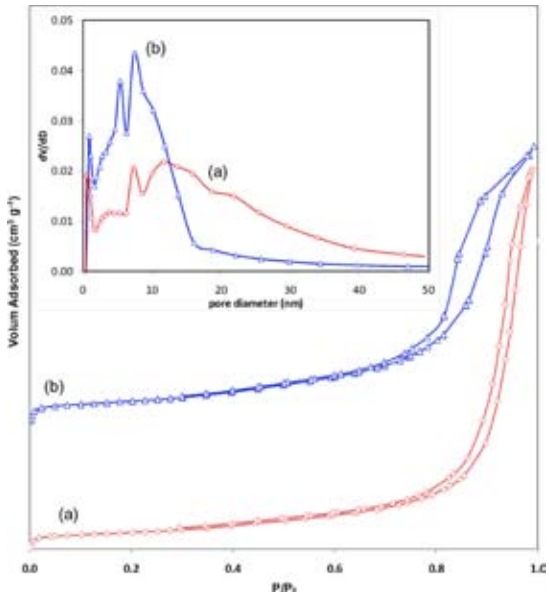

Fig. 4. The effect of NaOH (a) and KOH (b) on the Nitrogen adsorption/desorption isotherms and Pore-size distribution of mesoporous AlOOH.

purification. In a typical synthesis, 20 mmol of $Al(NO_3)_3 * 9H_2O$ was dissolved in 50 mL of deionized water with vigorous stirring. NaOH or KOH (2 Molar) was subsequently added drop by drop to the solution to give lacteous precipitates immediately. At this point, the pH value of the reaction mixture was ~12. The mixture was further stirred vigorously for 5 min before it was sealed into a 100 mL Teflon-lined stainless-steel autoclave, which was then placed and kept in the electric oven at 200 °C for 24 h. Thereafter the autoclave was allowed to cool to room temperature. The white resultant colloidal product was centrifuged and washed three times with deionized water, and then the product was dried at 60 °C for 24 h.

Characterization

The XRD patterns of the products were recorded using a B8 ADVANCE, BRUKER X-ray diffractometer with CuK α-radiation (λ = 1.54 Å). The crystallite sizes were estimated using the Scherrer equation:

$$D = 0.9\ \lambda/(\beta \cos \theta),$$

Where λ is the wavelength of X-rays, θ is the Bragg angle and β is the half-width of the diffraction peak.

Fourier transform infrared (FTIR) spectra were obtained on a WQF-510 FTIR, RAYLEIGH spectrometer. The morphologies of the samples were studied by field emission scanning electron microscopy (model S-4160, HITACHI). The nitrogen adsorption and desorption isotherms at −196 °C were measured with a MINI II-310, BEL SORP, BEL ANALYZER. Samples were degassed at 125 °C for 180 min before measurements. Specific surface areas and pore volume were determined by the Brunau-

er-Emmett-Teller (BET) model and pore size distributions were measured using BJH method.

Conclusions

Under similar condition, the effect of NaOH and KOH as precipitating agent on the synthesis of mesoporous AlOOH via a hydrothermal reaction route have been successfully presented. Comparative observations demonstrate that the precipitating agents play important roles in the form of AlOOH nanostructure. In the appropriate case of pH =12 and KOH as precipitating agent, the obtained samples are pure and crystalline with the high surface area 98 m^2/g and excellent porous properties. This condition for the synthesis of nano-structures has great significance for its simplicity, its high efficiency, and its good potential for catalyst, sorbents, ceramic and other fields.

Acknowledgements

The authors gratefully acknowledge Islamic Azad University, Kermanshah Branch for technical and financial supports.

References

1. Chen, Q.; Udomsangpetch, C.; Shen, S. C.; Liu, Y. C.; Chen, Z.; Zeng, X. T. *Thin Solid Films* **2009,** *517*, 4871-4874.
2. Zhu, Y.; Hou, H.; Tang, G.; Hu, Q., *Eur. J. Solid State Inorg. Chem.* **2010,** 872-878.
3. Zhang, L.; Jiao, X.; Chen, D.; Jiao, M., *Eur. J. Solid State Inorg. Chem.* **2011,** 5258-5264.
4. Hou, H.; Zhu, Y.; Tang, G.; Hu, Q., *Mater. Charact.* **2012,** *68*, 33-41.
5. Liu, L.; Huang, W.; Gao, Z. H.; Yin, L. H. *J. Ind. Eng. Chem.* **2012,** *18*, 123-127.
6. Peng, H.X.Z.; Fan, D.S.; Mudher, J.R.G.; Evans, *Mater. Sci. Eng. A* **2002,** *335*, 207-216.
7. Hellmig, R.J.H. F., *Phys. Stat. Sol. (a)* **1999,** *175*, 549-553.
8. Boumaza, A.; Favaro, L.; Lédion, J.; Sattonnay, G.; Brubach, J. B.; Berthet, P.; Huntz, A. M.; Roy, P.; Tétot, R. *J. Solid State Chem.* **2009,** *182*, 1171-1176.
9. Yu, Z. Q.; Wang, C. X.; Gu, X. T.; Li, C. *J. Lumin.* **2004,** *106*, 153-157.
10. Li, G.; Liu, Y.; Liu, D.; Liu, L.; Liu, C. *Mater. Res. Bull.* **2010,** *45*, 1487-1491.
11. Zhang, L.; Zhu, Y. J. *J. Phys. Chem. C* **2008,** *112*, 16764-16768.
12. He, T.; Xiang, L.; Zhu, W.; Zhu, S. *Mater. Lett.* **2008,** *62*, 2939-2942.
13. Li, Y.; Liu, J.; Jia, Z. *Mater. Lett.* **2006,** *60*, 3586-3590.
14. Chen, X. Y.; Zhang, Z. J.; Li, X. L.; Lee, S. W. *Solid State Commun.* **2008,** *145*, 368-373.
15. Cai, W.; Yu, J.; Mann, S. *Micropor. Mesopor. Mater.* **2009,** *122*, 42-47.
16. Zhang, L.; Lu, W.; Yan, L.; Feng, Y.; Bao, X.; Ni, J.; Shang, X.; Lv, Y. *Micropor. Mesopor. Mater.* **2009,** *119*, 208-216.
17. Liang, H.; Liu, L.; Yang, Z.; Yang, Y. *Cryst. Res. Technol.* **2010,** *45*, 195-198.
18. Alemi, A.; Hosseinpour, Z.; Dolatyari, M.; Bakhtiari, A. *Phys. Status Solidi B* **2012,** *249*, 1264-1270.
19. Chen, X. Y.; Lee, S. W. *Chem. Phys. Lett.* **2007,** *438*, 279-284.
20. Li, W.-J.; Shi, E.-W.; Zhong, W.-Z.; Yin, Z.-W. *J. Cryst. Growth* **1999,** *203*, 186-196.
21. Zhang, J.; Liu, S.; Lin, J.; Song, H.; Luo, J.; Elssfah, E.; Ammar, E.; Huang, Y.; Ding, X.; Gao, J. *J. Phys. Chem. B* **2006,** *110*, 14249-14252.
22. Musić, S.; Dragčević, Đ.; Popović, S. *Mater. Lett.* **1999,** *40*, 269-274.
23. Fu, G.-f.; Wang, J.; Xu, B.; Gao, H.; Xu, X.-l.; Cheng, H. *T. Nonferr. Metal. Soc.* **2010,** *20*, 221-225.
24. Feng, Y.; Lu, W.; Zhang, L.; Bao, X.; Yue, B.; lv, Y.; Shang, X. *Cryst. Growth Des.* **2008,** *8*, 1426-1429.
25. Sing, K. S. W.; Everett, D. H.; Haul, R. A. W.; Moscou, L.; Pierotti, R. A.; Rouquerol, J.; Siemieniewska, T. *Pure.App. Chem.* **1985,** *57*, 603-619.
26. Xu, B.; Wang, J.; Yu, H.; Gao, H. *J. Environ. Sci.* **2011,** *23*, 49-52.